Available online at www.sciencedirect.com

ScienceDirect

Journal of Taibah University for Science 10 (2016) 601–606

Journal of Taibah University for Science

www.elsevier.com/locate/jtusci

Hydrothermal synthesis of zinc stannate nanoparticles for antibacterial applications

J. Emima Jeronsia [a], L. Allwin Joseph [a], M. Mary Jaculine [b], P. Annie Vinosha [a], S. Jerome Das [a,*]

[a] *Department of Physics, Loyola College, Chennai 600034, India*
[b] *Department of Physics, Velammal Engineering College, Chennai 600066, India*

Received 24 November 2015; accepted 15 December 2015
Available online 29 December 2015

Abstract

A facile and economical hydrothermal method was used to synthesise Zn_2SnO_4 nanoparticles with cubic spinel structure. The crystallography and optical properties of the as-synthesised nanoparticles were studied using X-ray diffraction (XRD) and UV–visible spectroscopy (UV–vis). The morphology of the nanoparticles was observed using field emission scanning electron microscopy (FESEM). The synergistic antibacterial effect of Zn_2SnO_4 nanoparticles against Gram-positive and Gram-negative pathogenic bacteria was investigated. These results indicate that the Zn_2SnO_4 nanoparticles have potent antibacterial activity against both Gram-positive and Gram-negative bacteria and can be used as a bactericidal agent to prevent and control the spread and persistence of infectious diseases.

Keywords: Zinc stannate; Hydrothermal method; Antibacterial property

1. Introduction

Microbes and humans have forged a unique and largely beneficial relationship, but emerging infectious diseases continue to be one of the daunting challenges worldwide, leading to the upsurge in the investigation of nanomaterials. Given that the bacteria have developed resistance against many common antibacterial agents, there is a need for concrete advances in developing effective antibacterial therapeutic agents. Significant efforts have been directed towards the development of metal oxide nanoparticles, which are demonstrated to be effective for treating infectious diseases to combat antibiotic-resistant bacteria [1,2]. Recently, zinc-based stannate materials have attracted considerable

Abbreviations: XRD, X-ray diffraction; UV–vis, UV–visible spectroscopy; FT-IR, Fourier transform infrared spectroscopy; FESEM, field emission scanning electron microscopy; NZ, no zone; NPs, nanoparticles.

* Corresponding author. Tel.: +91 04428178200; fax: +91 04428175566.
E-mail address: jeromedas.s@gmail.com (S.J. Das).
Peer review under responsibility of Taibah University

Production and hosting by Elsevier

http://dx.doi.org/10.1016/j.jtusci.2015.12.003

attention due to their versatile applications in diverse fields, including photoelectrochemical cells, transparent conductive electrodes, Li-ion batteries, photocatalysts, and sensors [3–10]. Researchers have developed different techniques to synthesise zinc stannate nanostructures, which include solvothermal [11], high-temperature calcination [12], solution combustion [13], precipitation method [14], sol–gel [15], and hydrothermal reaction [5,7,16–19]. The hydrothermal synthesis has been demonstrated beyond doubt to be the most efficient method for growing zinc stannate nanostructures with various morphologies, such as cubes, spheres, and rods, by varying the chemicophysical parameters. Although the antibacterial behaviour of many metal oxides has been investigated, the studies on the antibacterial potential of zinc stannate nanoparticles are still at a nascent stage. Considering the potential toxicity of metal oxide nanoparticles to pathogenic bacteria, we report the antibacterial efficacy of Zn_2SnO_4 nanoparticles prepared via hydrothermal method. In this study, we investigated their structural and optical properties and their antibacterial activity against Gram-positive (*Staphylococcus aureus*, *Bacillus subtilis*) and Gram-negative (*Klebsiella pneumonia*, *Escherichia coli*) bacteria. To that end, this report describes the first systematic study on the antibacterial properties of Zn_2SnO_4 nanoparticles.

2. Materials and methods

2.1. Materials

Zinc chloride, tin chloride pentahydrate and sodium hydroxide (NaOH) were purchased from Sigma Aldrich. Double distilled water is used throughout the experiment.

2.2. Preparation of Zn_2SnO_4 nanoparticles

Zn_2SnO_4 nanoparticles were synthesised via hydrothermal method using NaOH as a mineraliser. In a typical procedure, the ratio of Zn:Sn:NaOH is 2:1:8. Zinc chloride and tin chloride pentahydrate were completely dissolved in double-distilled water to form a transparent solution under magnetic stirring for 3 h. NaOH was subsequently added drop-wise into the mixture to form a white slurry. The precursor solutions were maintained at a pH of 8. After stirring for 30 min, the final mixture was transferred into a Teflon line stainless steel autoclave with a filling capacity of 80%. The autoclave was maintained at 200 °C for 24 h and cooled naturally to room temperature. The resulting nanoparticles were separated from the reaction solution by centrifugation and washed repeatedly with deionized water and ethanol. Finally, the washed particles were dried at 80 °C for 20 h to obtain the powdered sample.

2.3. Analysis of Zn_2SnO_4 nanoparticles

The optical absorption spectra of Zn_2SnO_4 nanoparticles were obtained using a Perkin Elmer Lambda 25 UV-Vis spectrometer in the wavelength range of 200–800 nm. The as-synthesised NPs were pressed into a pellet, and FT-IR spectrum of the pellet was recorded in the region 4000–400 cm^{-1}. The X-ray diffraction patterns was recorded using a Rich Seifert diffractometer with monochromatic CuK_α ($\lambda = 1.5406$ Å) radiation in the 2θ range of 10–80°. The morphology of the ZnO and Zn_2SnO_4 nanoparticles was observed using a FESEM (Field emission scanning electron microscopy).

2.4. Antibacterial assay

The antibacterial activities of the as-synthesised Zn_2SnO_4 nanoparticles were evaluated using the quantitative well diffusion assay. All glassware, media, and reagents used for this test were sterilised in an autoclave at 121 °C for 15 min. The Mueller Hinton agar was used as a test medium for antibacterial susceptibility testing. Gram-positive (*S. aureus*, *B. subtilis*) and Gram-negative (*K. pneumonia*, *E. coli*) bacteria were used as the model test strains. Microbes were streaked on the plate surface using a sterile cotton swab. A sterile cork borer (8 mm diameter) was used to make five wells. The four different concentrations (250, 500, 750, and 1000 μg) of Zn_2SnO_4 nanoparticle suspension were filled in the wells. The well plates were incubated at 37 °C for 24 h, and they were examined for the effectiveness of Zn_2SnO_4 nanoparticles by measuring the zone of inhibition.

3. Results and discussion

The powder XRD pattern of the as-synthesised sample is shown in Fig. 1. The diffraction pattern matches notably well with the standard JCPDS powder diffraction file no. 24-1470. The pattern reveals the formation of face-centered cubic spinel structure with the lattice constant $a = 8.657$ Å. In a hydrothermal process, the alkaline concentration is a key factor that influences the crystallinity, morphology, and size of the as-synthesised sample [19]. The XRD pattern indicates that the reaction is complete and the as-synthesised nanoparticles are close to the expected stoichiometric ratio. The mean

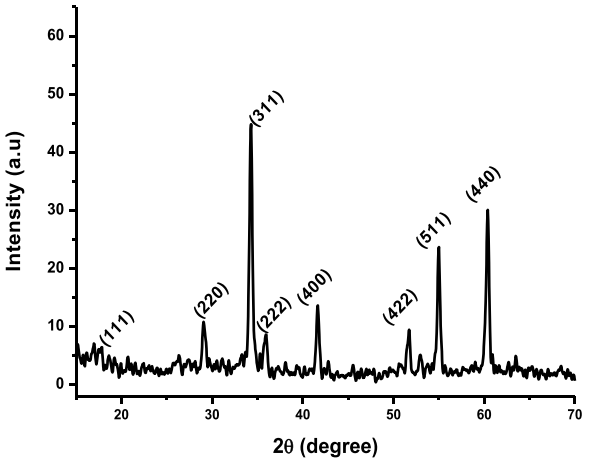

Fig. 1. X-ray diffraction spectrum (XRD) of Zn_2SnO_4 nanoparticles.

Table 1
Parameters calculated from XRD pattern of Zn_2SnO_4 nanoparticles.

Position (2θ)	hkl	d-spacing	Crystallite size (nm)
17.794	111	4.9806	17.79
29.073	220	3.0715	18.16
34.293	311	2.6149	22.07
35.858	222	2.5023	22.16
41.645	400	2.1687	22.56
51.659	422	1.7694	19.53
54.979	511	1.6701	23.77
60.406	440	1.53121	22.23

crystallite size was calculated using the Scherrer equation (1), given as

$$D = \frac{k\lambda}{\beta \cos\theta} \tag{1}$$

where D is the average grain size in nm, k (0.89) is a constant, λ is the X-ray wavelength, and θ and β are the diffraction angle and full-width at half-maximum of the observed peaks, respectively. From Table 1, the mean crystallite size is found to be 20.95 nm. Compared to other synthesis methods [20], highly crystalline powders with narrow size distribution and high purity can be obtained via hydrothermal synthesis route without any post treatment at high temperature, which makes it an excellent method to synthesise Zn_2SnO_4 nanoparticles.

UV–vis absorption spectrum was used to study the energy structures and optical properties of Zn_2SnO_4 NPs. The diffuse reflectance spectrum of Zn_2SnO_4 NPs shows a sharp increase in the reflectance at 300 nm, as seen in Fig. 2. The band gap energy was determined using the Kubelka–Munk function:

$$(h\nu F(R\infty))^2 = A(h\nu - E_g) \tag{2}$$

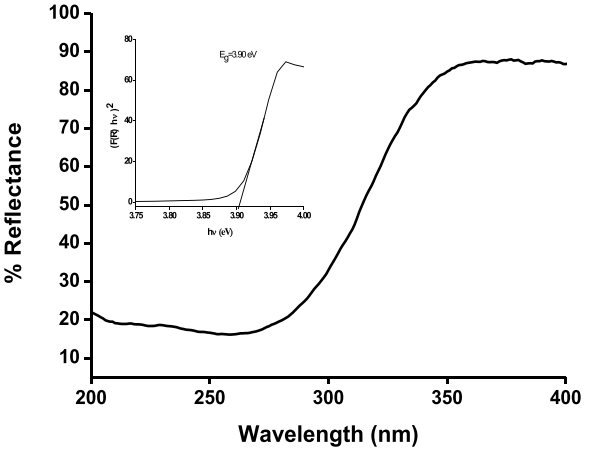

Fig. 2. Diffuse reflectance spectrum of Zn_2SnO_4 nanoparticles (UV–vis). Inset: Band gap energy plot.

where h is the Planck's constant, ν is the frequency of vibration, E_g is the energy gap, A is the proportionality constant, and $F(R\infty)$ is the function of reflectance:

$$F(R\infty) = \frac{(1-R)^2}{2R} \tag{3}$$

where (R) is the absolute value of reflectance and $F(R)$ is equivalent to the absorption coefficient. The direct band gap of Zn_2SnO_4 was estimated by plotting $(F(R)\cdot h\nu)^2$ vs $h\nu$ (eV) as shown in the inset of Fig. 2. The optical band gap of zinc stannate nanoparticles is found to be 3.9 eV, which is apparently larger than that of bulk zinc stannate (3.6 eV). This blue shift in the optical band gap is due to the quantum confinement effect arising from the small size. The fundamental band gap of zinc stannate with a direct-forbidden transition is proposed to be 3.6–3.7 eV, but upon heating the band gap narrows down to 3.25 eV due to the incorporation of excess Zn into the Zn_2SnO_4 crystal.

FT-IR spectrum was recorded for zinc stannate in the range 400–4000 cm^{-1} and is shown in Fig. 3. A broad absorption peak observed at 530–591 cm^{-1} is due to the symmetric stretching vibration of ZnO and SnO_2 groups, and this band could be assigned to the Sn–O–Zn bonding in the Zn_2SnO_4. The absorption peaks at ~1600 and 3280 cm^{-1} indicate the presence of hydrogen bonds and the absorption peak at ~1429 cm^{-1} is assigned to the C–H vibration mode attributed to the organic residuals. The peak at ~2243 cm^{-1} is assigned to the possible bonding of Zn in ZnO and the peak ~1170 cm^{-1} is attributed to the Sn–O stretching vibrations in Zn_2SnO_4. These observed peaks (at 530–591, ~1170, and ~2243 cm^{-1}) are attributed to the formation of Zn_2SnO_4.

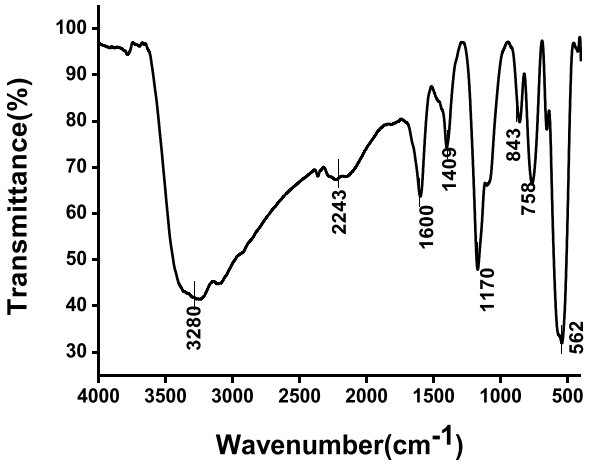

Fig. 3. Fourier transform infrared spectrum (FT-IR) of Zn_2SnO_4 nanoparticles.

The FESEM analysis was used to identify the morphology of the synthesised Zn_2SnO_4NPs. The SEM image of Zn_2SnO_4 nanoparticles shown in Fig. 4 reveals spherical morphology of the as-synthesised particles and the formation of network of aggregates. The growth of zinc stannate nanoparticles is initiated by the reaction between zinc ions and tin ions during hydrothermal synthesis. Apart from the reaction time and temperature, the concentration of sodium hydroxide in the precursor solution plays an important role in determining the size and shape of zinc stannate nanoparticles. Zinc hydroxystannate is transformed into zinc stannate at a medium concentration of sodium hydroxide.

3.1. Evaluation of antibacterial activity

In this study, the relative antibacterial activity of Zn_2SnO_4 nanoparticles with a mean crystallite size of 20.95 nm was investigated quantitatively by the well diffusion method. Table 2 shows the four different concentrations of Zn_2SnO_4 nanoparticle suspension tested against Gram-positive (*S. aureus*, *B. subtilis*) and Gram-negative (*K. pneumonia*, *E. coli*) bacteria. Based on the observations (Fig. 5), the presence of an inhibition zone clearly indicates the biocidal action of Zn_2SnO_4 nanoparticles. The size of the inhibition zone increases significantly with the increasing concentration of NPs. Zn_2SnO_4 NPs have the maximum antibacterial efficacy against Gram-positive *B. subtilis* with the highest zone of inhibition of 19 mm followed by a zone of inhibition of 18 mm *against S. aureus*. Moderate antibacterial activity against Gram-negative *K. pneumonia* and *E. coli* with lower zone of inhibition of 12 mm is observed. The toxicity of Zn_2SnO_4 NPs depends on their concentration and these NPs are mildly toxic at low concentration. The mechanism of nanoparticle toxicity depends on composition, size, surface modification, intrinsic properties, and bacterial species. NPs attach to the bacterial cell membrane by electrostatic interaction and disrupt the integrity of bacterial cell, which in turn increases its permeability leading to cell death. The toxicity induced due to dissolved Zn ions and Sn ions from Zn_2SnO_4 nanoparticles is negligible and the toxicity strength of NPs depends on intrinsic toxic properties of heavy metals [21].

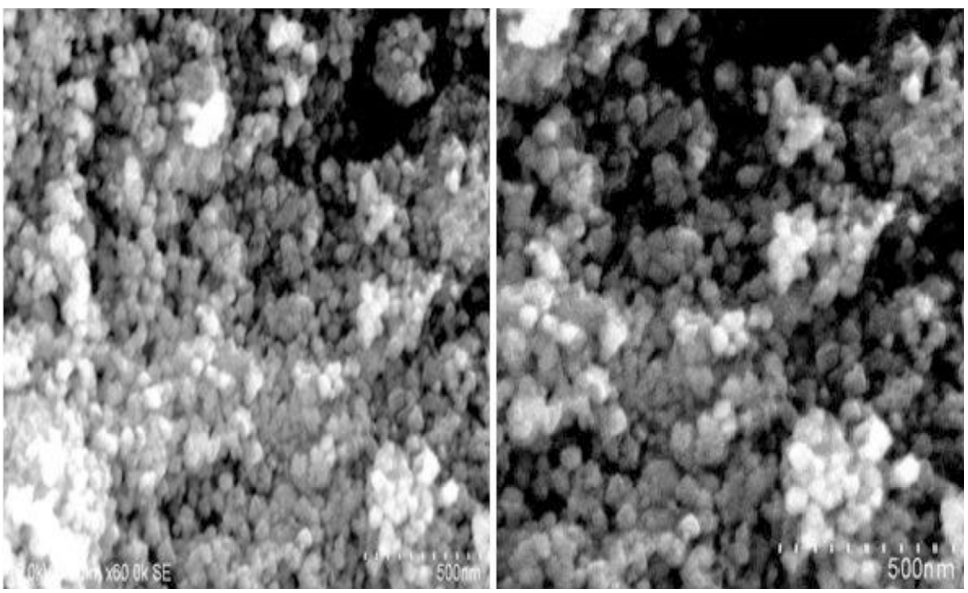

Fig. 4. Field emission scanning electron microscopy (FESEM) images of Zn_2SnO_4 nanoparticles.

Table 2
Antibacterial efficacy of as-synthesised Zn_2SnO_4 nanoparticles against human pathogenic bacteria (NZ – no zone).

Study no.	Bacterial strains	Zone of inhibition (mm) Concentration (μg/ml)				
		250	500	750	1000	Standard
1	*S. aureus*	11	13	15	18	14
2	*Bacillus subtilis*	16	17	18	19	13
3	*Klebsiella pneumonia*	NZ	NZ	11	12	14
4	*Escherichia coli*	NZ	NZ	11	12	14

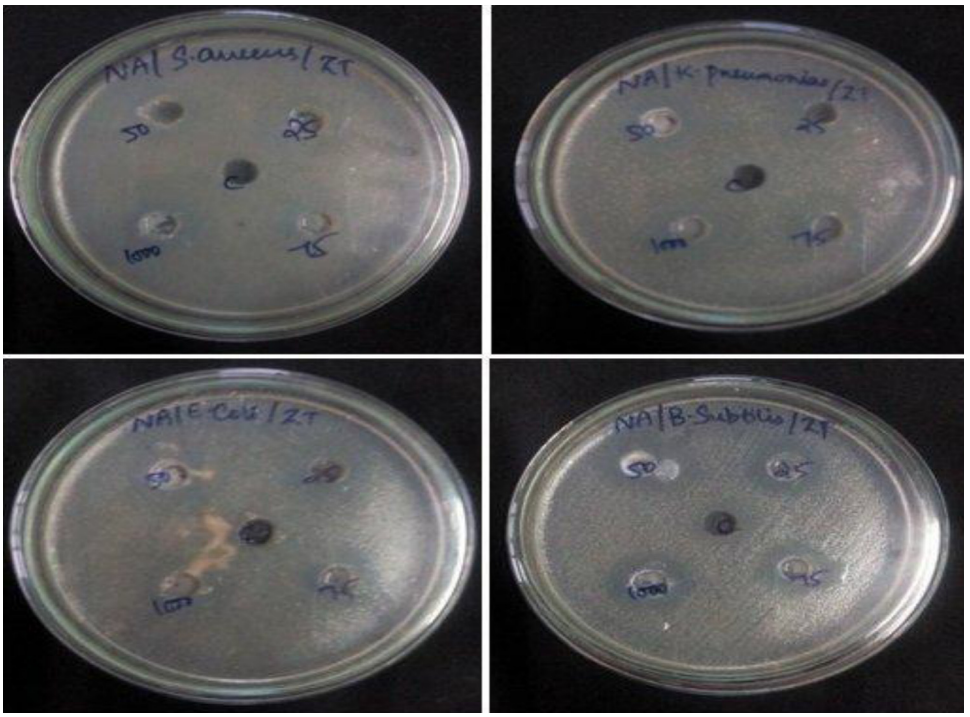

Fig. 5. Antibacterial efficacy of Zn_2SnO_4 nanoparticles against Gram-positive (*S. aureus*, *Bacillus subtilis*) and Gram-negative (*Klebsiella pneumonia*, *Escherichia coli*) bacteria.

4. Conclusions

Spherical Zn_2SnO_4 nanoparticles were successfully synthesized by hydrothermal method under mild reaction condition. The lattice parameters calculated from X-ray diffraction pattern revealed the formation of face-centered cubic spinel structured Zn_2SnO_4 with a mean crystallite size of 20.95 nm. The band gap energy calculated from the diffuse reflectance spectrum is 3.9 eV for Zn_2SnO_4 nanoparticles, which is slightly higher than the bulk value of 3.6 eV for Zn_2SnO_4. FT-IR studies revealed the different functional groups present in the as-synthesised Zn_2SnO_4 and further confirmed the formation of zinc stannate nanoparticles. Based on the test results, we can conclude that Zn_2SnO_4 nanoparticles exhibit efficient antibacterial activity, which makes them a promising candidate for biomedical and pharmaceutical applications.

Competing interests

The authors declare that they have no competing interests.

Authors' contributions

Emima and Allwin carried out experiments and wrote the manuscript. Emima, Allwin, Annie, Mary Jaculine, and Jerome Das discussed the experimental results and

commented on the manuscript. All authors read and approved the final manuscript.

Acknowledgements

The authors are thankful to the management of Loyola College, Chennai for providing the necessary facilities to carry out this research work and also acknowledge Armats BioteK Lab for helping out in the antibacterial test.

References

[1] M. Miyauchi, Z. Liu, Z.-G. Zhao, S. Anandan, K. Hara, Single crystalline zinc stannate nanoparticles for efficient photo electrochemical devices, Chem. Commun. 46 (2010) 1529–1531.

[2] P.K. Stoimenov, R.L. Klinger, G.L. Marchin, K.J. Klabunde, Metal oxide nanoparticles as bactericidal agents, Langmuir 18 (2002) 6679–6686.

[3] T. Lana-Villarreal, G. Boschloo, A. Hagfeldt, Nanostructured zinc stannate as semiconductor working electrodes for dye-sensitized solar cells, J. Phys. Chem. C 111 (2007) 5549–5556.

[4] B. Tan, E. Toman, Y. Li, Y. Wu, Zinc stannate (Zn_2SnO_4) dye-sensitized solar cells, J. Am. Chem. Soc. 129 (2007) 4162–4163.

[5] M.A. Alpuche-Aviles, Y. Wu, Photoelectrochemical study of the band structure of Zn_2SnO_4 prepared by the hydrothermal method, J. Am. Chem. Soc. 131 (2009) 3216–3224.

[6] G. Ma, R. Zou, L. Jiang, Z. Zhang, Y. Xue, L. Yu, G. Song, W. Lia, J. Hu, Phase-controlled synthesis and gas-sensing properties of zinc stannate ($ZnSnO_3$ and Zn_2SnO_4) faceted solid and hollow microcrystals, CrystEngComm 14 (2012) 2172–2179.

[7] A. Rong, X.P. Gao, G.R. Li, T.Y. Yan, H.Y. Zhu, J.Q. Qu, D.Y. Song, Hydrothermal synthesis of Zn_2SnO_4 as anode materials for Li-ion battery, J. Phys. Chem. B 110 (2006) 14754–14760.

[8] A. Sivapunniyam, N. Wiromrat, M.T.Z. Myint, J. Dutta, High-performance liquefied petroleum gas sensing based on nanostructures of zinc oxide and zinc stannate, Sens. Actuators B: Chem. 157 (2011) 232–239.

[9] Z. Li, Y. Zhou, J. Zhang, W. Tu, Q. Liu, T. Yu, Z. Zou, Hexagonal nanoplate-textured micro-octahedron Zn_2SnO_4: combined effects toward enhanced efficiencies of dye-sensitized solar cell and photoreduction of CO_2 into hydrocarbon fuels, Cryst. Growth Des. 12 (2012) 1476–1481.

[10] S.-H. Choi, D. Hwang, D.-Y. Kim, Y. Kervella, P. Maldivi, S.-Y. Jang, R. Demadrille, I.-D. Kim, Amorphous zinc stannate (Zn_2SnO_4) nanofibers networks as photoelectrodes for organic dye-sensitized solar cells, Adv. Funct. Mater. 23 (2013) 3146–3155.

[11] G. Sun, S. Zhang, Y. Li, Solvothermal synthesis of Zn_2SnO_4 nanocrystals and their photocatalytic properties, Int. J. Photoenergy (2014), 7 pp.

[12] J.-B. Shi, P.-F. Wu, H.-S. Lin, Y.-T. Lin, H.-W. Lee, C.-T. Kao, W.-H. Liao, S.-L. Young, Synthesis and characterization of single-crystalline zinc tin oxide nanowires, Nanoscale Res. Lett. 9 (2014) 210.

[13] P. Jayabala, V. Sasirekha, J. Mayandi, V. Ramakrishnan, Microwave assisted synthesis of zinc stannate nanocubes for dye sensitized solar cell application, Superlattices Microstruct. 75 (2014) 775–784.

[14] A.R. Babar, S.B. Kumbhar, S.S. Shinde, A.V. Moholkar, J.H. Kim, K.Y. Rajpure, Structural, compositional and electrical properties of co-precipitated zinc stannate, J. Alloys Compd. 509 (2011) 7508–7514.

[15] Y. Zhao, L. Hu, H. Liu, M. Liao, X. Fang, L. Wua, Band gap tunable Zn_2SnO_4 nanocubes through thermal effect and their outstanding ultraviolet light photoresponse, Sci. Rep. 4 (2014) 6847.

[16] X. Lou, X. Jia, J. Xu, S. Liu, Q. Gao, Hydrothermal synthesis, characterization and photocatalytic properties of Zn_2SnO_4 nanocrystal, Mater. Sci. Eng. A 432 (2006) 221–225.

[17] E.L. Foletto, J.M. Simões, M.A. Mazutti, S.L. Jahn, E.I. Muller, L.S.F. Pereira, E.M. de Moraes Flores, Application of Zn_2SnO_4 photocatalyst prepared by microwave-assisted hydrothermal route in the degradation of organic pollutant under sunlight, Ceram. Int. 39 (2013) 4569–4574.

[18] Z. Chen, M. Cao, C. Hu, Novel Zn_2SnO_4 hierarchical nanostructures and their gas sensing properties toward ethanol, J. Phys. Chem. C 115 (2011) 5522–5529.

[19] V. Šepelák, S.M. Becker, I. Bergmann, S. Indris, M. Scheuermann, A. Feldhoff, C. Kübel, M. Bruns, N. Stürzl, A.S. Ulrich, M. Ghafari, H. Hahn, C.P. Grey, K.D. Beckerbk, P. Heitjans, Nonequilibrium structure of Zn_2SnO_4 spinel nanoparticles, J. Mater. Chem. 22 (2012) 3117–3126.

[20] N. Musee, M. Thwala, N. Nota, The antibacterial effects of engineered nanomaterials: implications for wastewater treatment plants, J. Environ. Monit. 13 (2011) 1164–1183.

[21] G. Applerot, J. Lellouche, N. Perkas, Y. Nitzan, A. Gedanken, E. Banin, ZnO nanoparticle-coated surfaces inhibit bacterial biofilm formation and increase antibiotic susceptibility, RSC Adv. 2 (2012) 2314–2321.